

Antinematic local order in dendrimer liquids

Ioannis A. Georgiou,¹ Primož Ziherl,^{2,3} and Gerhard Kahl⁴

¹*Institute for Theoretical Physics, Technische Universität Wien,
Wiedner Hauptstraße 8-10, A-1040 Vienna, Austria*

²*Faculty of Mathematics and Physics, University of Ljubljana, Jadranska 19, SI-1000 Ljubljana, Slovenia*

³*Jozef Stefan Institute, Jamova 39, SI-1000 Ljubljana, Slovenia*

⁴*Institute for Theoretical Physics and Center for Computational Materials Science,
Technische Universität Wien, Wiedner Hauptstraße 8-10, A-1040 Vienna, Austria*

(Dated: July 22, 2022)

We use monomer-resolved numerical simulations to study the positional and orientational structure of a dense dendrimer solution, focusing on the effects of dendrimers' prolate shape and deformability on the short-range order. Our results provide unambiguous evidence that the nearest-neighbor shell of a tagged particle consists of a mixture of crossed, side-by-side, side-to-end, and end-to-end pair configurations, imposing *antinematic* rather than nematic order observed in undeformable rod-like particles. This packing pattern persists even at densities where particle overlap becomes sizable. We demonstrate that the antinematic arrangement is compatible with the A15 crystal lattice reported in several dendrimer compounds.

PACS numbers: 47.57.J-, 61.20.-p, 61.20.Ja

Dendrimers are highly branched macromolecules with a tree-like structure. This particular architecture is the result of a controlled, step-by-step synthesis where – starting from a pair of bonded, tri-functional monomers – the macromolecule grows by adding core monomers generation by generation. The outermost, so-called shell monomers can be decorated by suitable end groups. The first report on synthesis of dendrimers by the Vögtle group in 1978 [1] received little attention but the interest in these materials increased considerably after their potential applications were pointed out [2].

With a compact convex shape determined by their architecture, dendrimers are in many ways more similar to colloidal particles than to spread-out, random-coil linear polymers – yet they are penetrable like random coils such that two dendrimers can overlap to a high degree. Much like colloidal particles, dendrimers readily crystallize but many lattices observed (e.g., A15 and σ phases [3, 4]) are untypical for classical colloids. Some aspects of this unique behavior may be related to the dendrimer shape: The early-generation dendrimers can be viewed as prolate ellipsoids, the molecular elongation decreasing with the generation number (cf. Fig. 5 of Ref. [5]). Although smaller than in linear polymers [6], the aspect ratio of dendrimers is still quite large and may exceed 4 in the first (i.e., innermost) generation [7].

It is natural to expect that the optimal packing mode of dendrimers will depend on their shape and deformability. Indeed, atomistic simulations revealed that at large densities considerable interpenetration does take place [8] leading to the A15 cubic lattice as seen experimentally. Complementary to this prediction are theoretical studies of penetrable ellipsoids. If forced into alignment, they form elongated lattices (obtained, e.g., by stretching the body-centered cubic crystal along [001], [110], or [111]

direction) rather than cubic lattices [9, 10].

To better understand the complex interplay of their deformation and reorientation, it is worthwhile to develop a coarse-grained description of dendrimers where they are regarded as soft anisometric particles. In this Letter, we use monomer-resolved numerical simulations to investigate the short-range structure of a dendrimer liquid, and we interpret the results in terms of dendrimer shape, anisotropic positional order, and orientational order. We find that dendrimers align such that the long axes of most nearest neighbors are perpendicular, e.g., $\mathbf{I} - \cdot \mathbf{I} - \mathbf{I}$ (where dots represent rods pointing into or out of the paper). This so-called antinematic local packing pattern [11] is robust and reveals a new and deeper insight into the structure of dendrimer crystals.

The model dendrimers studied here are based on tri-functional monomers interacting with the Morse potential and the bonds between them are represented by the finitely extensible nonlinear elastic (FENE) potential [Eqs. (2) and (1) of Ref. [12], respectively]. The core monomers are different from the shell monomers, the main differences being the deeper attractive well and the shorter bond length. The parameters of the potentials are listed in Table I using the notation of Ref. [12]; unless indicated otherwise all results reported here pertain to the ($G = 4$) dendrimers.

Standard *NVT* Monte Carlo simulations are used to obtain the equilibrium structure of a single dendrimer, a dendrimer pair, and an ensemble of 27 dendrimers in a cubic box. Starting from several independent initial configurations at high temperatures, we cooled the system using a simulated annealing protocol to reach the desired temperature T such that $k_B T$ is $1.4\epsilon_{CC}$, ϵ_{CC} being the depth of the core-core attractive potential. The simulation runs typically involved 5×10^5 equilibration sweeps

	Morse			FENE		
	ϵ	ad_{CC}	d/d_{CC}	Kd_{CC}^2	l^0/d_{CC}	R/d_{CC}
CC	0.714	6.4	1.00	40	1.8750	0.3750
CS	0.014	19.2	1.25	20	2.8125	0.5625
SS	0.014	19.2	1.50			

Table I: Parameters of the core-core (CC), core-shell (CS), and shell-shell (SS) intermonomer Morse potential (ϵ , a , and d) and of the core-core and core-shell FENE bonds (K , l^0 , and R) [see Eqs. (2) and (1) of Ref. [12]] in our dendrimers. Lengths are given in units of d_{CC} whereas ϵ is in units of $k_B T$.

followed by 5×10^7 to 5×10^8 production sweeps with a sampling frequency between 5×10^3 and 5×10^4 sweeps as suitable. The positions of monomers were recorded and used to evaluate the structural features.

We quantify the shape of dendrimers by computing the radius of gyration tensor $\mathcal{S}_{ik} = \langle x_i x_k \rangle$, where x_i is the i -th coordinate of a monomer in the dendrimer's center-of-mass system, and the average is over all monomers in a dendrimer and over 2×10^4 and 2×10^5 frames for a single dendrimer and for a pair, respectively. From the eigenvalues of \mathcal{S} , denoted by E_1 , E_2 , and E_3 and arranged in descending order, we compute the dendrimer asphericity and acylindricity

$$b = \frac{E_1 - (E_2 + E_3)/2}{R_g^2} \quad \text{and} \quad c = \frac{E_2 - E_3}{R_g^2}, \quad (1)$$

respectively [6, 13]; the radius of gyration is defined by $R_g^2 = E_1 + E_2 + E_3$. For spherical particles, b and c vanish. Although not the only possible choice of shape measures [14], asphericity and acylindricity clearly show that isolated dendrimers are non-axisymmetric, prolate ellipsoids which become increasingly more spherical as G is increased. In *isolated* ($G = 2$)-dendrimers $b = 0.35 \pm 0.12$ and $c = 0.15 \pm 0.07$ (corresponding to semiaxes ratio of 1.67:1.28:1) whereas ($G = 10$)-dendrimers are almost spherical ($b = 0.061 \pm 0.012$ and $c = 0.022 \pm 0.014$) [15].

The effective potential of dendrimers and their shape must be strongly interrelated. The solid line in Fig. 1 shows the effective interaction energy, $\beta\Phi_{\text{eff}}(r)$, of two ($G = 4$)-dendrimers in the zero-density limit computed using umbrella sampling [16]. The pair potential can be approximated by the generalized exponential model of index ≈ 2.6 (GEM-2.6) [17] suggesting that the dendrimers may form clusters of overlapping particles [18]. Also plotted in Fig. 1 are the dendrimer asphericity and acylindricity as functions of the center-to-center distance. We observe a sizeable increase of asphericity b of $\approx 22\%$ for $1.5 \lesssim r/R_g^0 \lesssim 2.5$, R_g^0 being the radius of gyration of an isolated dendrimer. On the other hand, the acylindricity c essentially does not deviate from its value in isolated particles. Concomitantly, one observes in this r -range an increase in the effective interaction of $\approx 30\%$ of the potential at complete overlap $\beta\Phi_{\text{eff}}(r = 0)$. These observations imply both in terms of shape and in terms of

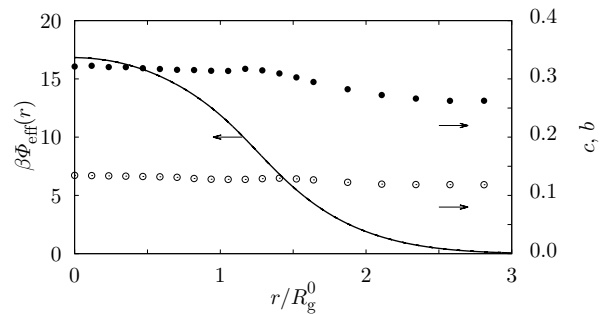


Figure 1: Effective potential, $\beta\Phi_{\text{eff}}(r)$, of a pair of ($G = 4$)-dendrimers (solid line), and their asphericity, b , and acylindricity, c (filled and open circles, respectively, both shown on the secondary vertical axis) vs. center-to-center separation.

energy that the dendrimers start to penetrate into each other for $1.5 \lesssim r/R_g^0 \lesssim 2.5$.

We now focus on the anisotropic positional and orientational order at close separations. Since acylindricity c is small in all cases explored here, we only monitor the orientation of the dendrimers' long axes relative to the center-to-center vector (Fig. 2a). Despite this reduction of parameters, the various configurations of two dendrimers can still be described by three angles and therefore a detailed representation of the pair distribution is rather impractical. Instead, we choose to characterize each configuration of two dendrimers using

$$\alpha = \frac{1}{2} \left[(\hat{\epsilon}_1 \cdot \hat{\mathbf{r}})^2 + (\hat{\epsilon}_2 \cdot \hat{\mathbf{r}})^2 \right], \quad (2)$$

where $\hat{\epsilon}_1$ and $\hat{\epsilon}_2$ are the directional unit vectors of the long axes of the dendrimers and $\hat{\mathbf{r}}$ is the unit center-to-center vector (Fig. 2a). Note that α is symmetric with respect to an interchange of dendrimers ($1 \leftrightarrow 2$) as well as to replacing $\hat{\epsilon}_i$ by $-\hat{\epsilon}_i$, reflecting thereby properly the headless nature of the dendrimers. The mapping of the relative orientation of $\hat{\epsilon}_1$, $\hat{\epsilon}_2$, and $\hat{\mathbf{r}}$ onto α is not unique as illustrated by six characteristic configurations shown in the table in Fig. 2b [19] along with their respective values of α . Additional insight into the relative arrangement of dendrimers is provided by the orientational order parameter

$$S = \frac{1}{2} (3 \cos^2 \theta - 1), \quad (3)$$

where θ is the angle between the long axes (Fig. 2a) and angular brackets denote ensemble average. Since the relative orientation of two dendrimers depends on r , so does S , and as illustrated by the table in Fig. 2b it distinguishes between some configurations with the same α (e.g., \parallel and \perp). In a pair of perfectly parallel or antiparallel dendrimers, $S = 1$ whereas in dendrimers oriented perpendicular to each other $S = -0.5$ (Fig. 2b).

In the following we discuss the conditional distribution function $P(r, \alpha)$ and the orientational order parameter

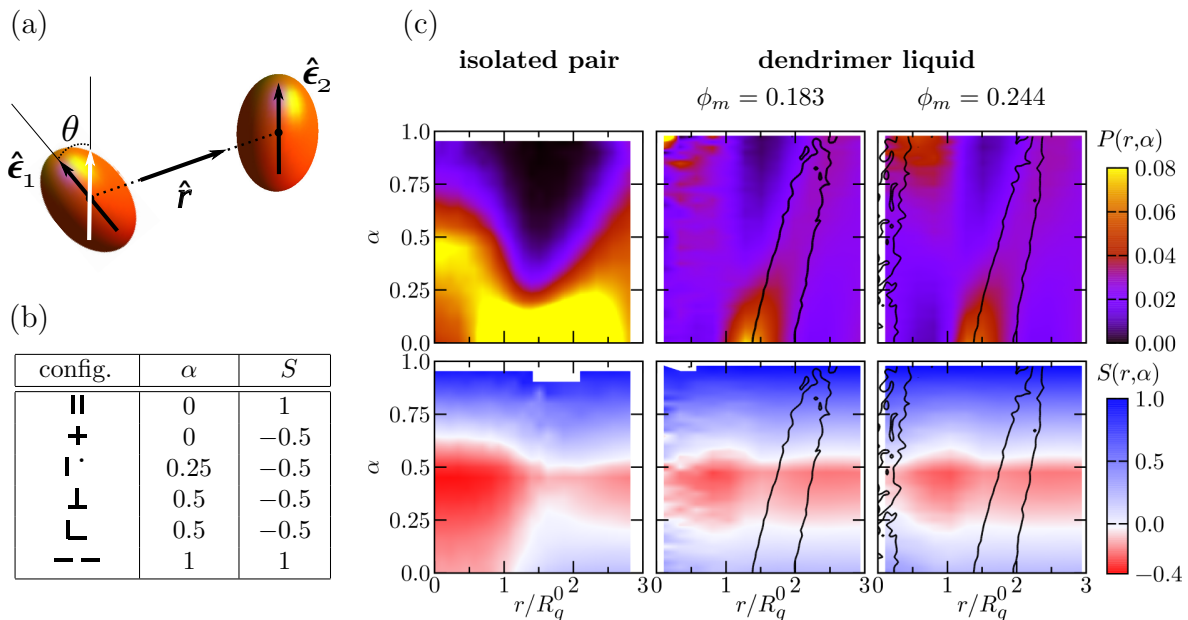


Figure 2: Positional and orientational order of two interacting dendrimers. Panel (a) shows two unit vectors, $\hat{\epsilon}_1$ and $\hat{\epsilon}_2$, needed to describe the respective orientations of two dendrimers represented by axisymmetric ellipsoids, θ being the angle between $\hat{\epsilon}_1$ and $\hat{\epsilon}_2$ such that $\cos\theta = \hat{\epsilon}_1 \cdot \hat{\epsilon}_2$ and \hat{r} being the unit center-to-center vector. Six characteristic pair configurations are listed in panel (b) along with the corresponding values of α and S [see Eqs. (2) and (3)]. Density plots of conditional distribution function $P(r, \alpha)$ and of the orientational order parameter S are presented in the top and bottom row, respectively; also shown are color codes. The left column of panel (c) shows data for the isolated pair whereas the middle and the right columns represent the liquid state at packing fractions $\phi_m = 0.183$ and $\phi_m = 0.244$, respectively [20]. Black contours are isolines of the pair distribution function $g(r; \alpha)$ at a value a little smaller than the height of the nearest-neighbor peak.

S for an isolated pair of dendrimers and a pair of dendrimers in a bulk liquid. The relative orientation of an isolated pair depends quite dramatically on their separation (left column of Fig. 2c). The flat profile of $P(r, \alpha)$ at $r/R_g^0 \gtrsim 3$ (not shown) indicates that at large separations the orientations of the dendrimers are completely uncorrelated such that all orientations of $\hat{\epsilon}_1$ and $\hat{\epsilon}_2$, are equally probable at any r that is large enough. However, as dendrimers penetrate into each other the correlations becomes more and more pronounced: As r/R_g^0 drops below ≈ 2.5 , $P(r, \alpha)$ peaks at $\alpha = 0$ and at $r/R_g^0 \approx 1.5$ the probability for configurations with $\alpha \lesssim 0.25$ is essentially negligible. In the regime of partial penetration for $1.5 \lesssim r/R_g^0 \lesssim 2.5$, the range of α where $P(r, \alpha)$ is enhanced coincides with the region of positive orientational order parameter (bottom-left panel of Fig. 2c), indicating thus the presence of || configurations. The regime of full overlap at $r/R_g^0 \lesssim 1$ is characterized by a somewhat broader distribution of $P(r, \alpha)$ peaking at $\alpha \approx 0.4$ and excluding the occurrence of states with large α ($\gtrsim 0.6$). Together with the strongly negative orientational order parameter S at small r , this implies that overlapping dendrimers show a strong preference to form \perp and \lfloor configurations (which are indistinguishable from the \oplus configuration as $r \rightarrow 0$). Thus we conclude that repulsion between the overlapping dendrimers forces them into

a perpendicular arrangement.

In a bulk liquid, the relative orientation of a pair is modified by the local structure. The middle column of Fig. 2c shows the conditional distribution function $P(r, \alpha)$ (top panel) and the orientational order parameter S at a packing fraction $\phi_m = 0.183$ [20]; both are strikingly different from their counterparts in two isolated dendrimers. In total, the variations of $P(r, \alpha)$ are less pronounced than in the case of an isolated pair. We note that (i) at the onset of dendrimer-dendrimer interaction at $r/R_g^0 \approx 2.5$, there is a slight preference for large- α configurations (e.g., --); (ii) at intermediate distances $r/R_g^0 \approx 1.5$ the $\alpha < 0.25$ configurations are favored and those with large α are increasingly more disfavored just like for the isolated pair; and (iii) overlapping dendrimers ($r \rightarrow 0$) prefer configurations with α close to 1, e.g. --.

The differences of the relative orientation of a pair of dendrimers in isolation and in a bulk liquid at both small and large separations [(i) and (iii)] are even more pronounced at the larger packing fraction $\phi_m = 0.244$ (right column of Fig. 2c) where particle overlap is rather substantial. This can be readily seen from the pair distribution function $g(r; \alpha)$ represented by an isoline which is superposed onto the plots of $P(r, \alpha)$ and S ; the value of $g(r; \alpha)$ on the isoline is a little smaller than the height of the nearest-neighbor peak. This representation is more

transparent than a comprehensive set of isolines and more robust than displaying only the exact location of the nearest-neighbor peak. At any given α , the position of the peak is located roughly halfway between by the respective small- r and the large- r points on the isoline.

At the smaller packing fraction $\phi_m = 0.183$ (middle column of Fig. 2c), the tilted $g(r; \alpha)$ isoline shows that the distance between the nearest $\alpha = 0$ neighbors is about $1.7R_g^0$; this corresponds to the **||** configuration since the negative $S = -0.5$ of the **+** configuration is inconsistent with the observed positive value of S (bottom-center panel in Fig. 2c). In contrast, the distance between neighbors in the end-to-end **---** configuration with $\alpha = 1$ is about $2.25R_g^0$. The intermediate- α configurations (**I'**, **I**, and **L**) are located at a distance of about $2R_g^0$. The relative orientation of two interacting dendrimers in a liquid at the larger packing fraction $\phi_m = 0.244$ is qualitatively similar except for the finite probability that the dendrimers overlap witnessed by the occurrence of isolines at small r -values. Since for small r the conditional distribution function $P(r, \alpha)$ peaks at $\alpha = 0$, we conclude that in a bulk liquid overlapping dendrimers are preferentially oriented parallel to each other.

Panel (a) of Fig. 3 shows an idealized schematic view of the local structure of the dendrimer liquid. The dendrimers are represented by axisymmetric ellipsoids of aspect ratio of 1.49, consistent with the average ratio of semiaxes of a single isolated dendrimer (Fig. 1). In the equatorial plane, the central reference dendrimer is surrounded by **||**, **I'**, and **I** neighbors, with the **||** neighbors being located a little closer to the reference particle than the **I'** and the **I** neighbors. The polar regions are populated either by **I** neighbors or by **---** neighbors, the latter being somewhat farther from the reference particle than the former. The resulting pattern is thus *antinelastic* [11] rather than nematic, and it has some reminiscence to the unusual simple monoclinic packing of hard ellipsoids [21] stable at aspect ratios larger than about 2, i.e., particles that are slightly more elongated than our dendrimers.

The distinct differences between $P(r, \alpha)$ for an isolated pair and a pair in a bulk dendrimer liquid (top row of Fig. 2c) are a clear signature of many-body effects. Equally telling is the comparison of the panels in the bottom row of Fig. 2c showing the orientational order of the dendrimers. In the case of an isolated pair the overlapping dendrimers are arranged perpendicular to each other (**+**) as witnessed by the extended red region in the bottom-left panel in Fig. 2c. In contrast, in a bulk liquid they are arranged end-to-end (**---**) as argued above. Such a strong effect would not be possible unless the local "cage" of neighbors were tight and ordered enough, leaving little space for a perpendicular orientation of overlapping dendrimers.

Based on these observations we can formulate our expectations for the structure of dendrimer crystals at even

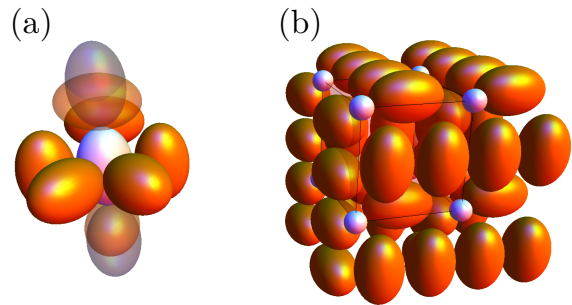


Figure 3: Schematic view of the antinelastic packing pattern observed in a dendrimer liquid (a). The nearest-neighbor shell around the reference particle (white ellipsoid) contains **||** (left and right), **I'** (back), and **I** (front) configurations in the equatorial region. The polar regions may be occupied either by **I** or **---** configurations (gray semitransparent ellipsoids), the latter being a little farther from the reference particle. Panel (b): The A15 lattice decorated by ellipsoids arranged in three sets of mutually interlocking columns is indeed able to capture the antinelastic nature of the pattern shown in panel (a); the dodecahedral interstitial sites (small white spheres only shown in the unit cell for clarity) lack a preferred orientation.

higher packing fractions. As the average orientation of dendrimers with a local antinelastic order is fairly isotropic, a crystalline lattice formed by dendrimers is likely highly symmetric, i.e., cubic. However, the single-site-type cubic lattices (e.g., simple, body-centered, and face-centered) are incompatible with the antinelastic order, implying that dendrimer crystals must be more complex. An obvious candidate is the A15 lattice [3, 4] based on three sets of mutually perpendicular columns of particles which accommodate many features of the packing pattern (Fig. 3b) discussed above. Each columnar site (ellipsoids in Fig. 3b) has **||** neighbors and hybrids of **I'**, **I**, and **L** neighbors as well as the more distant **---** neighbors. Thus, unlike any single-site cubic crystal structure, the A15 lattice is essentially very consistent with antinelastic order although the interstitial sites (small white spheres in Fig. 3b) are characterized by a dodecahedral environment and are most easily populated by spherical rather than elongated particles. In all, our results suggest that the stability of the A15 lattice is directly related to the elongated shape and deformability of dendrimers.

Furthermore, our investigations provide for the first time unambiguous evidence about the origin of the antinelastic order itself. In contrast to hard rodlike particles where excluded-volume interactions induce the *nematic* phase [23], we identify the softness and the anisotropy of the particles as *the* key mechanisms that are responsible for *antinelastic* particle arrangements. The dramatic change of the behavior due to softness is very much reminiscent of the many differences between the phase diagrams of hard and soft spheres [9, 17, 22].

We are indebted to Ronald Blaak (Wien), Hiroshi Noguchi (Tokyo), Silvano Romano (Pavia), and Gregor Skačej (Ljubljana) for many helpful suggestions. This work was supported by the Marie-Curie Initial Training Network COMPLOIDS (FP7-PEOPLE-ITN-2008 Grant No. 234810), by the Slovenian Research Agency (Grant No. P1-0055), and by the Austrian Science Fund (FWF) under Project No. F41 (SFB ViCoM).

-
- [1] E. Buhleier, W. Wehner, and F. Vögtle, *Synthesis* **1978**, 155 (1978).
- [2] D. A. Tomalia, H. Baker, and J. Dewald, *Polym. J.* **17**, 117 (1985).
- [3] V. S. K. Balagurusamy, G. Ungar, V. Percec, and G. Johansson, *J. Am. Chem. Soc.* **119**, 1539 (1997).
- [4] X. Zeng, G. Ungar, Y. Liu, V. Percec, A. E. Dulcey, and J. K. Hobbs, *Nature* **428**, 157 (2004).
- [5] P. M. Maiti, T. Çağın, G. Wang, and W. A. Goddard III, *Macromolecules* **37**, 6236 (2004).
- [6] K. Šolc, *J. Chem. Phys.* **55**, 335 (1971).
- [7] A. M. Naylor, W. A. Goddard III, G. E. Kiefer, and D. A. Tomalia, *J. Am. Chem. Soc.* **111**, 2339 (1989).
- [8] Y. Li, S.-T. Lin, and W. A. Goddard III, *J. Am. Chem. Soc.* **126**, 1872 (2004).
- [9] S. Prestipino and F. Saija, *J. Chem. Phys.* **126**, 194902 (2007).
- [10] A. Nikoubashman and C. N. Likos, *J. Phys.: Condens. Matter* **22**, 104107 (2009).
- [11] K. Sokalski and Th. W. Ruijgrok, *Physica A* **126**, 280 (1984).
- [12] B. M. Mladek, G. Kahl, and C. N. Likos, *Phys. Rev. Lett.* **100**, 028301 (2008).
- [13] D. N. Theodorou and U. W. Suter, *Macromolecules* **18**, 1206 (1985).
- [14] J. Rudnick and G. Gaspari, *J. Phys. A* **19**, L191 (1986).
- [15] Dendrimer shape may also be expressed in terms of $\delta = 1 - 3(E_1E_2 + E_2E_3 + E_3E_1)/(E_1 + E_2 + E_3)^2$ introduced in Ref. [14]. The values of δ for our dendrimers ($\delta = 0.172, 0.097$, and 4.38×10^{-3} for $G = 2, 4$, and 10 , respectively) are similar to those reported in poly(amido amide) [5] and poly(propylene imine) dendrimers [N. Zacharopoulos and I. G. Economou, *Macromolecules* **35**, 1814 (2002)].
- [16] D. Frenkel and B. Smit, *Understanding Molecular Simulation: From Algorithms to Applications* (Academic Press, San Diego, 2002).
- [17] B. M. Mladek, D. Gottwald, G. Kahl, M. Neumann, and C. N. Likos, *Phys. Rev. Lett.* **96**, 045701 (2006).
- [18] C. N. Likos, *Phys. Rep.* **348**, 267 (2001).
- [19] The orientation of the center-to-center unit vector is given implicitly in all of these configurations except **I** where we assume that the angle between the vertical dendrimer and the center-to-center vector is 45° like in the **L** configuration.
- [20] The packing fraction $\phi_m = V_m/V$ is defined as the bare volume of monomers V_m divided by the total volume V ; in the ($G = 4$)-dendrimer $V_m = N_D \pi (30d_{CC}^3 + 32d_{SS}^3)/6$ with N_D, d_{CC} , and d_{SS} being the number of dendrimers and the diameters of the core and shell monomers, respectively [D. Lenz, R. Blaak, and C. N. Likos, *Soft Matter* **5**, 2905 (2009)].
- [21] M. Radu, P. Pfeiderer, and T. Schilling, *J. Chem. Phys.* **131**, 164513 (2009).
- [22] J. C. Pàmies, A. Cacciuto, and D. Frenkel, *J. Chem. Phys.* **131**, 044514 (2009); **131**, 159903 (2009).
- [23] P. Bolhuis and D. Frenkel, *J. Chem. Phys.* **106**, 666 (1997).